Alloying effect of tungsten on the structural and magnetic properties of CoCrFeNiW high entropy alloys

Raquel Lizárraga,[1,*] Erik Holmström,[2] and Levente Vitos[1,3,4]

[1]*Applied Materials Physics, Department of Materials Science and Engineering, Royal Institute of Technology (KTH), Stockholm SE-10044, Sweden*

[2]*Sandvik Coromant R&D, Stockholm SE-12680, Sweden*

[3]*Department of Physics and Astronomy, Division of Materials Theory, Uppsala University, Box 516, SE-75121 Uppsala, Sweden*

[4]*Research Institute for Solid State Physics and Optics, Wigner Research Center for Physics, Budapest H-1525, P.O. Box 49, Hungary*

The recent observation of the hexagonal-closed-packed (hcp) phase in CoCrFeNi-based multicomponent alloys has reopened the question of phase stability in these alloys. We investigate the alloying effect of tungsten on the crystal and magnetic structures of $(CoCrFeNi)_{1-x}W_x$ high entropy alloys using density functional theory by means of the exact muffin-tin orbital method. The body-centered-cubic (bcc), face-centered-cubic (fcc), and hcp phases are investigated in two magnetic states: ferrimagnetic and paramagnetic. Below 8 at. % W the ground state of $(CoCrFeNi)_{1-x}W_x$ is the ferrimagnetic hcp phase and above that, the ferrimagnetic bcc phase is stabilized. Our calculations show that the fcc and hcp phases are energetically very close in the whole range of studied W compositions and because CoCrFeNi and $(CoCrFeNi)_{0.93}W_{0.07}$ are observed in the fcc phase at room temperature, the hcp-fcc structural phase transition is expected to occur at lower temperatures. The total magnetic moment in bcc is almost double the value calculated for the fcc and hcp structures, which is due to that Cr moments are nearly quenched in bcc but are coupled antiferromagnetically to Fe, Ni, and Co in both hcp and fcc. We calculated also the Curie temperature of these alloys using the mean-field approximation. The calculated value was found to be 155 K for fcc CoCrFeNi, in excellent agreement with experiments, and the addition of W decreases this value. Our results contribute to the development of these relatively unknown corrosion-resistant materials into industrial applications, such as cemented carbides.

I. INTRODUCTION

High entropy alloys (HEAs) are defined in general as multicomponent alloys consisting of five or more principal elements in compositions, typically ranging between 5 and 35 atomic percent [1]. This virtually unexplored class of new alloys offers an enormous span of material possibilities due to the vast number of different combinations of elements to design innovative engineering materials with tunable properties. HEAs often exhibit superior mechanical properties such as high strength at high temperatures [1–3], ductility [4], toughness [5], and resistance to corrosion [6,7], wear [8], and fatigue [9]. Despite the diversity of their components, these complex alloys can form simple single phases and are often stabilized in bcc and fcc phases [4,10]. The observation of the hcp phase has been more elusive; however, recently, there have been reports of the stabilization of the hcp phase in CoCrFeMnNi [11], AlHfScTiZr [12], Al$_{0.5}$CoCrFeNi [13], and CoCrFeNi [14]. The last two HEAs have long been viewed as fcc systems.

CoCrFeNi is an interesting material that has been extensively studied in the past [14–21]. Recently, CoCrFeNi with dissolved W and C has been considered for replacing cobalt in cemented carbides because of its good mechanical properties

[22]. Cemented carbides are composite materials that are constituted by a hard phase: tungsten carbide grains cemented or glued by a metallic binder phase, typically Co. The use of cemented carbides is quite universal. They are employed in metal cutting, structural parts, mining and construction, wear parts, etc., which makes cemented carbides very important materials for industry. Due to health concerns related to Co dust [23–25], the substitution or reduction of Co content in cemented carbides has become urgent. Unfortunately, despite a lot of research efforts in the last decades, this issue has not been solved satisfactorily [26].

The task is to identify a Co property that correlates with its good performance as a binder to be able to emulate this property in the alternative material [27]. For example, it is known in Co-based alloys that the resistance to galling, a form of wear, is related to the low stacking fault energy (STE) [28] and that tensile properties are associated to the fcc-hcp phase transition [29]. Recently, an *ab initio* and thermodynamic study on SFE and its relation to the fcc-hcp phase transition in Co-based binary alloys showed that, when Co is alloyed with Fe or Ni the fcc phase is stabilized, whereas Cr and W (below 10% W) stabilize the hcp [27]. Consequently, CoCrFeNi is considered a good candidate to replace Co in cemented carbides because the hcp and fcc phases are energetically close and therefore SFEs are likely to be as low as in Co and other Co-based alloys [27]. Because W dissolves in the binder phase, it is a key issue to understand the effect of W on

*raqli@kth.se

the phase stability of CoCrFeNi. Understanding the magnetic properties of these HEAs is also very important if they are going to be used as a replacement for Co in cemented carbides because the change of the magnetic response of Co due to the presence of W in the binder is widely used in industry to control the quality of cutting tools in a nondestructive manner [30].

There are very few investigations in the literature on these (CoCrFeNi)$_{1-x}$W$_x$ alloys [7,22,31]. Poletti *et al.* synthesized new CoCrNiFeW$_{0.3}$ and CoCrNiFeW$_{0.3}$ + 5 at. % of C alloys and were able to demonstrate that the performance of these new HEAs compare well with that of benchmark commercial alloys, Stellite6, as wear resistance materials for coating automotive engine valves [31]. Altogether, (CoCrFeNi)$_{1-x}$W$_x$ HEAs are important engineering materials for several applications and their further development depends critically on a better understanding of their properties. The present study aims at investigating the effect of W on the phase stability and the magnetic properties of (CoCrFeNi)$_{1-x}$W$_x$ HEA by means of first-principles theory. We compare our results with pure Co to determine to which extent these HEAs behave as Co. The paper is organized as follows: in Sec. II we describe the computational methods, in Sec. III we present structural and magnetic analyses based on our *ab initio* calculations and, finally, we summarize our findings in Sec. IV.

II. COMPUTATIONAL DETAILS

We performed total-energy calculations in the framework of density functional theory (DFT) [32,33] as implemented in the exact muffin-tin orbital (EMTO) method [34–37]. EMTO is an improved screened Korringa-Kohn-Rostoker (KKR) method [38], where the exact one-electron potential is represented by large overlapping muffin-tin potential spheres. By using overlapping spheres the exact crystal potential can be described more accurately when compared to the conventional muffin-tin or not overlapping approaches [36,39]. The Perdew-Burke-Ernzerhof generalized gradient approximation (PBE) was used for the exchange correlation functional [40]. HEA can be stabilized in random solid solutions. In this study the chemical disorder in the random solid solutions was treated within the coherent-potential approximation (CPA) [41–46]. Nowadays, CPA is one of the most powerful techniques to treat random alloys due to the possibility to calculate properties of materials accurately using the unit cell instead of employing large and time consuming supercells [37]. The latter method has the advantage of being able to consider local relaxations, [47] however, for the properties investigated in this study local relaxations appeared not to be significant.

The EMTO method together with CPA have been successfully applied to calculate the ground state properties of ordered [48,49] and disordered alloys [50] as well as HEA [19,51,52]. The full charge density (FCD) technique is implemented for accurate total energies [53,54]. The EMTO basis includes *s*, *p*, *d* and *f* orbitals. The one-electron equations were solved within the scalar relativistic approximation and the soft-core scheme [37]. The total number of k-points in the irreducible Brilloiun zone was 506, 916 and 1919 points for the bcc, fcc and hcp lattice. The screening parameter was kept constant throughout the calculations, 0.6020.

III. RESULTS AND DISCUSSIONS

A. HCP phase

We investigate the crystal structure of the high entropy alloys (CoCrFeNi)$_{1-x}$W$_x$, where the W concentration varies between 0 to 10 at.%. This concentration range was chosen because it is in the relevant interval where W diffusion occurs in the binder phase of cemented carbides. Two magnetic states were considered here: ferrimagnetic and paramagnetic. The ferrimagnetic state corresponds to a spin arrangement where the spin of Cr atoms aligns opposite to all the other spins of the other elements in the alloy. The paramagnetic state is modeled by using the disordered local moments (DLM) approach that in combination with CPA treats CoCrFeNiW as a 50-50 alloy, where (CoCrFeNiW)$_{50}^{\uparrow}$ (CoCrFeNiW)$_{50}^{\downarrow}$ with magnetic moments distributed randomly [55].

When stabilized in simple solid solution, HEAs are often found in the bcc or fcc structure [10]. However, there have been recent reports on the observation of the hcp phase in CoCrFeMnNi [11], AlHfScTiZr [12], and even in Al$_{0.5}$CoCrFeNi [13] and CoCrFeNi [14] HEA. Our present calculations show that the hcp structure is energetically close to fcc, similar to the case of pure Co [56]. In order to investigate the hcp phase, we searched for the equilibrium values of the c/a ratio and the lattice constant a for each composition 0, 2, 4, 6, 8, and 10 at. % W. We utilized a dense mesh (15 × 10) of c/a and a values. The calculated total-energy surfaces were then fitted using the following polynomial expression:

$$E(y = c/a, z = a) = a_1 y^3 + a_2 y^2 + a_3 z^2 + a_4 y + a_5 z, \tag{1}$$

where the coefficients a_1, a_2, a_3, a_4, and a_5 as well as the equilibrium values of c/a and a are listed in Table I for each composition and for pure hcp Co for comparison. The total-energy surfaces fitted using Eq. (1) and energy contours are displayed in Fig. 1(a) for hcp CoCrFeNi and Fig. 1(b) for pure hcp Co. Total-energy surfaces and energy contours for (CoCrFeNi)$_{1-x}$W$_x$ with $x > 0$ were also calculated. We do not show them here since they are very similar to the energy surface of CoCrFeNi [Fig. 1(a)] [57].

In Fig. 1 we compare hcp CoCrFeNi with pure hcp Co and find striking similarities between the two energy surfaces. The shape of both curves is very alike and exhibits little variation around the minima, in particular, along the c/a axis. The inset in the figure displays the energy difference between the two energy surfaces at $c/a = 1.62$.

Table I shows that there is a nearly linear increase of the lattice constant as the concentration of W increases, whereas the value of c/a stays almost constant. Interestingly, c/a is slightly larger for pure Co than for (CoCrFeNi)$_{1-x}$W$_x$.

B. Phase stability

In this section we present the results of total-energy calculations for the bcc, fcc, and hcp structures. For the hcp structure we have used the equilibrium values for c/a and a listed in Table I. Figure 2 displays the total energies for the concentration range between 0 and 10 at. % W in the ferrimagnetic and paramagnetic state. The ferrimagnetic hcp phase is energetically more stable than fcc and bcc in both

TABLE I. Coefficients a_1, a_2, a_3, a_4, and a_5 used in Eq. (1) for $(CoCrFeNi)_{1-x}W_x$ HEAs. Equilibrium lattice parameters and c/a ratios for all compositions. Experimental values are taken from Ref. [58].

x (at. %)	a_1 (Ry/Å^3)	a_2 (Ry/Å^2)	a_3 (Ry/Å^2)	a_4 (Ry/Å)	a_5 (Ry/Å)	c/a	a (Å)
Co (Expt.)						1.623	2.5071
Co (Theor.)	−5757.13	688.15	8984.4	−3583.75	1227.83	1.624	2.50
0	−4912.97	581.91	7670.56	−3046.05	1047.47	1.621	2.51
2	−4969.72	582.18	7759.82	−3064.53	1059.49	1.621	2.52
4	−5273.26	611.76	8232.72	−3235.50	1124.34	1.621	2.53
6	−5593.14	644.37	8739.91	−3423.00	1191.54	1.621	2.55
8	−5946.84	680.92	9301.37	−3631.83	1265.77	1.622	2.56
10	−6342.41	722.61	7670.56	−3046.05	1047.47	1.623	2.57
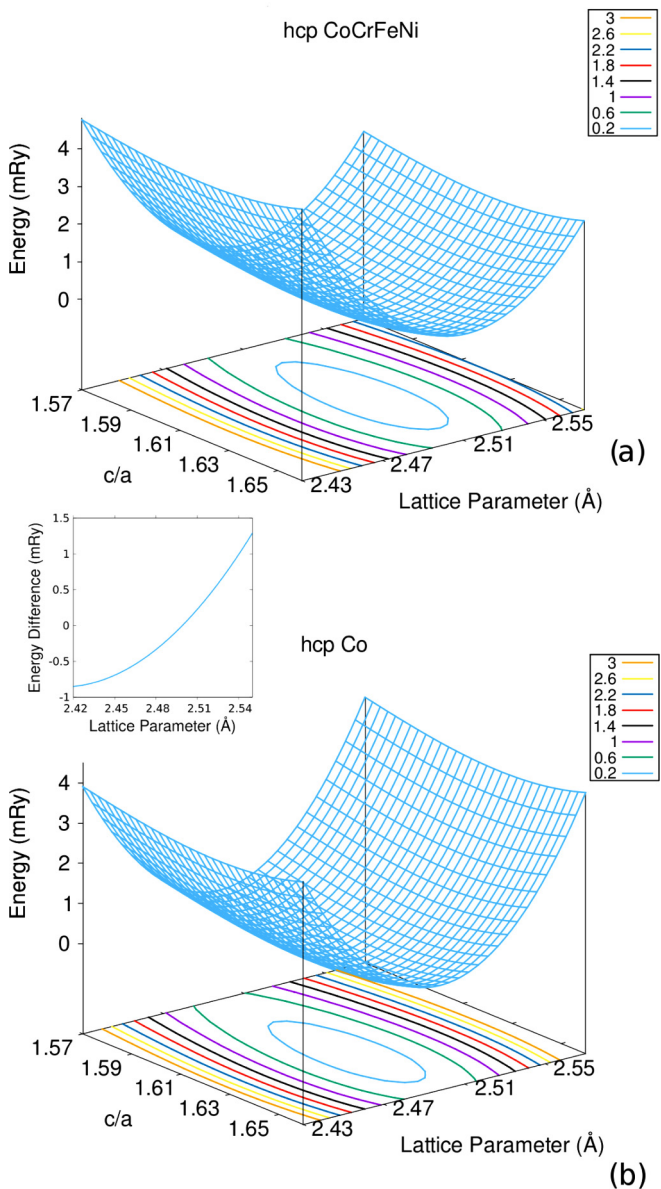
FIG. 1. Total energy surfaces for (a) CoCrFeNi and (b) pure Co in the hcp structure as a function of the c/a ratio and lattice constant a. Energy contours are also displayed. In both cases a ferrimagnetic state was assumed. The inset shows the energy difference between hcp CoCrFeNi and pure hcp Co energy surfaces at $c/a = 1.62$.

ferrimagnetic and paramagnetic states for compositions below 8 at. % W. Total energy differences for the ferrimagnetic state are listed with respect to the energy of the hcp phase at the equilibrium volume in Table II. The ferrimagnetic hcp and fcc phases are almost degenerate with an energy difference of 0.2–0.4 mRy for concentrations below 6 at. % W. This difference becomes even smaller as the concentration of W increases above 8 at. % W and at 10 at. % W the two curves are almost on top of each other. Above 8 at. % W the ferrimagnetic bcc phase becomes the global minimum. The
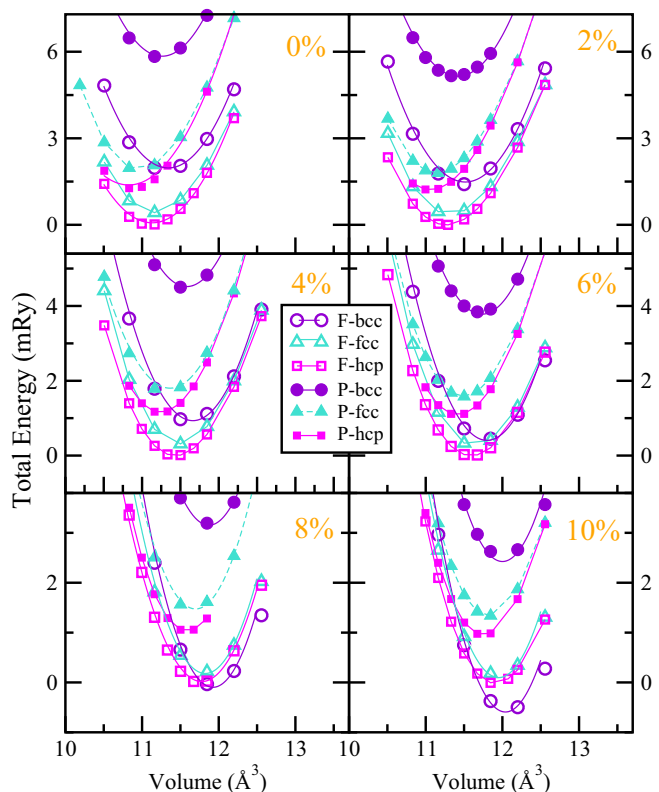
FIG. 2. Total energy for $(CoCrFeNi)_{1-x}W_x$ where $x = 0, 2, 4, 6, 10$ at. % W. The label F denotes a ferrimagnetic configuration in which all the atomic spins point in one direction except Cr, whose spin aligns opposite to the rest (open symbols). The label P corresponds to the paramagnetic state. In all cases the total energy is given with respect to the energy of the ferrimagnetic hcp structure (open squares).

TABLE II. Total-energy differences given with respect to the hcp phase at the equilibrium volume.

x (at. %)	$\Delta E_{\text{bcc-hcp}}$ (mRy)	$\Delta E_{\text{fcc-hcp}}$ (mRy)
0	1.89	0.40
2	1.40	0.37
4	0.91	0.31
6	0.43	0.26
8	0.05	0.21
10	−0.56	0.14

ferrimagnetic bcc phase favors larger equilibrium volumes than both hcp and fcc.

Paramagnetic solutions are always higher in energy than the ferrimagnetic ones and their equilibrium volumes are smaller than their ferrimagnetic counterparts. The paramagnetic bcc energy curve lies well above all the other curves and the paramagnetic fcc and hcp curves have an almost constant energy difference of ∼0.5 mRy across the whole range of W concentrations.

It is interesting to notice that the energy difference between ferrimagnetic hcp and fcc is smaller than in the case of pure Co, that is ∼1.6 mRy [56]. This suggests that the hcp ⇄ fcc transition temperature is lower than in the case of pure Co, 700 K [58]. Recently, Niu *et al.* observed the presence of a nanostructure with hcp phase in CrCoNi [59]. They calculated also the free-energy difference between hcp and fcc by using DFT calculations and obtained ∼0.7 mRy, which is in the order of magnitude of the energy differences obtained here. We also notice that the fcc paramagnetic state energy is never lower than paramagnetic hcp, an effect that is also observed on pure Co [56]. This implies that magnetic effects alone cannot account for the phase transition and as it has been demonstrated for pure Co, several energy contributions, namely, vibrational energy, volume expansion effects, and magnetic and electronic entropy, may be needed to trigger the fcc-hcp phase transition in these multicomponent alloys.

The equilibrium volumes for the high entropy alloys $(CoCrFeNi)_{1-x}W_x$ have been obtained by minimization of the total-energy curves in Fig. 2. Figure 3 presents the equilibrium volumes for fcc, hcp, and bcc against concentration in the ferrimagnetic and paramagnetic state. One can observe that there is a linear increment of the equilibrium volumes as a function of W concentration with a similar slope 7.0–7.7×10^{-2} Å^3/at. % for all the investigated cases. The paramagnetic equilibrium volumes are always smaller than the ones corresponding to ferrimagnetic configurations. Ferrimagnetic hcp and fcc equilibrium volumes are very close for all concentrations. This resembles the pure Co case as well, where the volume change at the phase transition $\Delta V/V = 3.3 \times 10^{-3}$ is very small [60].

There is very little experimental work on these alloys, $(CoCrFeNi)_{1-x}W_x$. Poletti *et al.* synthetized and characterized $(CoCrFeNi)_{0.93}W_{0.07}$ by means of x-ray diffraction (XRD) and scanning electron microscopy (SEM) [31]. They found that the $(CoCrFeNi)_{0.93}W_{0.07}$ alloy is almost entirely constituted by an fcc phase once equilibrium is reached at room temperature and the lattice constant was determined
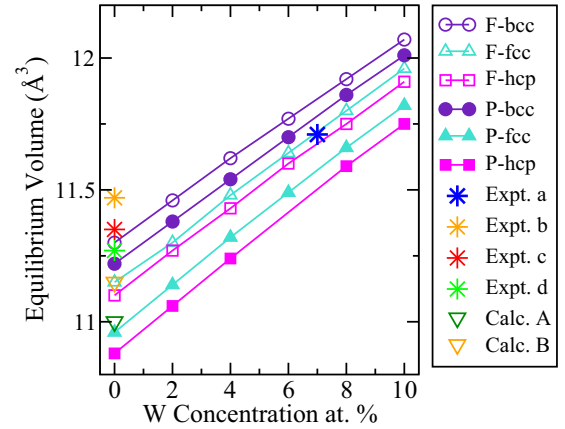
FIG. 3. Equilibrium volumes for $(CoCrFeNi)_{1-x}W_x$ in the bcc, fcc, and hcp structures considering the ferrimagnetic (open symbols) and paramagnetic state (full symbols). Experiments a, b, c, and d correspond to Refs. [31,15,16,65], respectively. Calculations A and B correspond to Refs. [51] and [19], respectively.

to be $3.6048 \pm 2 \times 10^{-4}$ Å ($V_{\text{at}} = 11.71$ Å^3). This is in excellent agreement with our calculated equilibrium volume, 11.713 Å^3, of the fcc phase in the ferrimagnetic state at 7 at. % W obtained by linear extrapolation of the FM fcc curve in Fig. 3. The value for paramagnetic fcc at 7 at. % W is 11.57 Å^3.

C. Magnetism

In this section we discuss the magnetic structure of $(CoCrFeNi)_{1-x}W_x$ HEAs. Figure 4 displays the atomic magnetic moments for Co, Cr, Fe, and Ni for each W concentration and for each crystalline phase. The moments are obtained at the equilibrium volume for each structure in the ferrimagnetic state. One can see that, in general, the magnetic moments of all elements are larger in the bcc phase, which can be seen as well in other CoCrFeNi-based HEAs [19,52,61]. Increasing the concentration of W does not change very much the atomic magnetic moments of the elements, except for Ni, where the magnetic moment decreases with a similar slope $\approx -7 \times 10^{-3} \mu_B$/at. % for all three phases.

Co magnetic moments in $(CoCrFeNi)_{1-x}W_x$ HEAs are slightly lower than in pure Co, and they tend to decrease as W concentration increases; conversely Fe slightly increases its magnetic moment with W concentration. The magnetic moments of Cr behave differently. In bcc, Cr has a very small magnetic moment, and only marginally increases with W concentration, whereas in hcp and fcc, Cr magnetic moments are negative varying between $-1 \mu_B$ and $-0.85 \mu_B$. This is the reason that in the bcc phase the total magnetic moment of the alloys is much larger than in hcp and fcc, where the Cr magnetic moments couples antiparallelly with the other spins. It is worth mentioning that there has been a report of a tendency of Cr-Cr repulsion in CoCrFeNi that might be related to the presence of short-range ordering at ambient temperatures [62]. However, since investigating this possibility would require a supercell approach and it is out of the scope of this paper we did not study this issue.
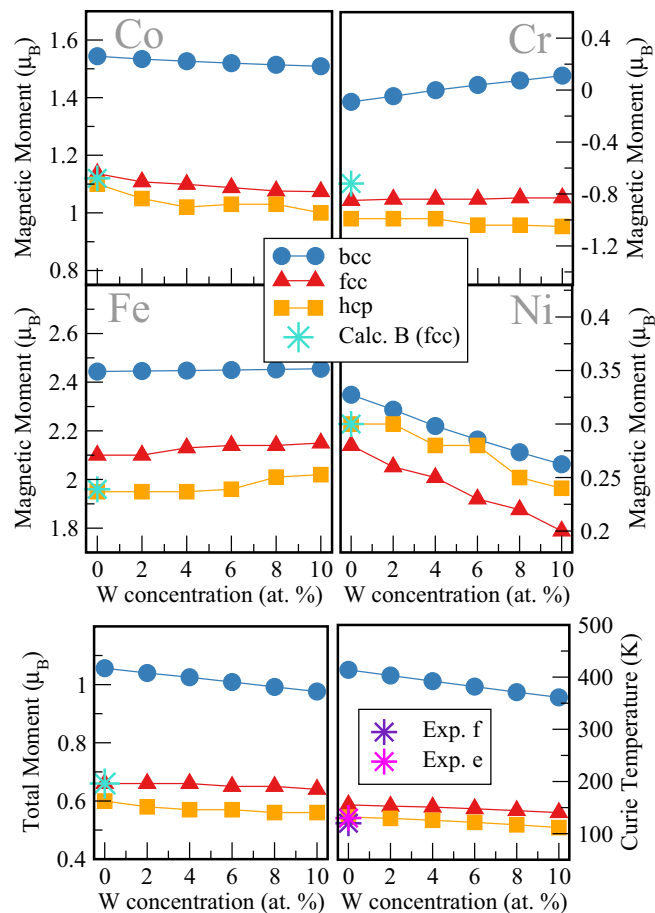
FIG. 4. Top panels: Co, Cr, Fe, and Ni atomic magnetic moments as a function of W concentration in the bcc, fcc, and hcp phases. Bottom panels: Total magnetic moment calculated for bcc, fcc, and hcp phases as a function of W concentration. Curie temperature as a function of W concentration. Expt. e and f and Calc. B correspond to Refs. [65,66,19], respectively.

In the bottom part of Fig. 4 we also show the total magnetic moment for $(CoCrFeNi)_{1-x}W_x$ as a function of W concentration. The effect of W is to decrease the total magnetic moment of the three phases, bcc, fcc, and hcp. The total magnetic moment of the bcc phase is nearly double the total magnetic moments of both fcc and hcp.

The magnetic saturation is commonly used in industry to assess the tungsten concentration in Co binders by means of a linearly decreasing magnetic saturation as function of W content [63,64]. In Fig. 4, we notice that the magnetic response of CoCrFeNi also behaves linearly on the W content, similarly to that of a Co binder.

The last graph in Fig. 4 displays the Curie temperature (T_c) versus W concentration for bcc, fcc, and hcp. We have employed a mean-field expression [61]

$$T_c = \frac{2}{3}\frac{\left(E_{tot}^{DLM} - E_{tot}^{FM}\right)}{k_B(1 - c_W)}, \quad (2)$$

where E_{tot}^{DLM} and E_{tot}^{FM} are the total energies of the DLM and ferromagnetic states, respectively. Our calculated value

of the Curie temperature for CoCrFeNi in the fcc phase is 155 K, which compares remarkably well with experimental values 120–130 K [65,66] and other *ab initio* calculations [67,68]. Our *ab initio* trend predicts a decrease of T_c as the concentration of W increases. The effect is more pronounced on the bcc phase. Unfortunately, to our knowledge there are no experimental data to verify these trends.

IV. CONCLUSIONS

In this study we have calculated the phase stability and magnetic properties of $(CoCrFeNi)_{1-x}W_x$ HEAs. Calculations were performed for paramagnetic and ferrimagnetic states. In the latter, Cr magnetic moments are aligned in opposite direction to Fe, Co, and Ni. The paramagnetic state was modeled by using the DLM approach. The ground state of these HEAs is the ferrimagnetic hcp phase for concentrations below 8 at. % W and above it, the ferrimagnetic bcc phase becomes more stable. The ferrimagnetic hcp and fcc phase are energetically very close as in Co and Co-binary alloys. The calculated equilibrium volume of the fcc phase at 7 at. % W is in excellent agreement with the experimental value at room temperature.

Incrementing W concentration reduces the magnetic moment of Co and Ni, while it increases the Fe atomic moment. The total magnetic moment of these alloys is reduced with the increment of W concentration. The magnetic moment of Cr changes depending on the crystal structure; in bcc Cr moments are nearly quenched, however in fcc and hcp Cr magnetic moments are coupled antiferromagnetically to the other elements in these alloys. This accounts for the large difference in the total magnetic moment between bcc and the other two phases, hcp and fcc. Our calculated value of the Curie temperature of CoCrFeNi agrees well with experiments and the trend predicted by our calculations is that W decreases T_c.

In general, our results show that $(CoCrFeNi)_{1-x}W_x$ HEAs behave similarly to pure Co below 6 at. % W, where the fcc and hcp phases are very close in energy and hence stacking fault energies are likely to be small. The magnetic response of these multicomponent alloys follows the same trend as pure Co with increment of W. All these facts support the choice of CoCrFeNiW with less than 6 at. % W as a replacement for Co in cemented carbides and also encourage more experimental work on these corrosion-resistant materials for their further development as highly relevant materials for industrial applications.

[1] J.-W. Yeh, S.-K. Chen, S.-J. Lin, J.-Y. Gan, T.-S. Chin, T.-T. Shun, C.-H. Tsau, and S.-Y. Chang, Adv. Eng. Mater. **6**, 299 (2004).

[2] Y. Zhang, X. Yang, and P. K. Liaw, JOM **64**, 830 (2012).

[3] O. N. Senkov, J. M. Scott, S. V. Senkova, D. B. Miracle, and C. F. Woodward, J. Alloys Compd. **509**, 6043 (2012).

[4] Y. Zhang, T. T. Zuo, Z. Tang, M. C. Gao, K. A. Dahmen, P. K. Liaw, and Z. P. Lu, Prog. Mater. Sci. **61**, 1 (2014).

[5] B. Gludovatz, A. Hohenwarter, D. Catoor, E. H. Chang, E. P. George, and R. O. Ritchie, Science **345**, 1153 (2014).

[6] C. P. Lee, Y. Y. Chen, C. Y. Hsu, J. W. Yeh, and H. C. Shih, Thin Solid Films **517**, 1301 (2008).

[7] C. Shang, E. Axinte, J. Sun, X. Li, P. Li, J. Du, P. Qiao, and Y. Wang, Mater. Des. **117**, 193 (2017).

[8] M.-H. Chuang, M.-H. Tsai, W.-R. Wang, S.-J. Lin, and J.-W. Yeh, Acta Mater. **59**, 6308 (2011).

[9] M. A. Hemphill, T. Yuan, G. Y. Wang, J. W. Yeh, C. W. Tsai, A. Chuang, and P. K. Liaw, Acta Mater. **60**, 5723 (2012).

[10] B. S. Murty, J. W. Yeh, and S. Ranganathan, *High-Entropy Alloys* (Elsevier Science, London, 2014).

[11] C. L. Tracy, P. Park, D. R. Rittman, S. J. Zinkle, H. Bei, M. Lang, R. C. Ewing, and W. L. Mao, Nat. Commun. **8**, 15634 (2017).

[12] Rogal, P. L. Bobrowski, F. Körmann, S. Divinski, F. Stein, and B. Grabowski, Sci. Rep. **7**, 2209 (2017).

[13] J. Wang, Y. Zhang, S. Z. Niu, W. Y. Wang, H. C. Kou, and J. S. Li, MRS Commun. **7**, 879 (2017).

[14] F. X. Zhang, S. Zhao, K. Jin, H. Bei, D. Popov, C. Park, J. C. Neuefeind, W. J. Weber, and Y. Zhang, Appl. Phys. Lett. **110**, 011902 (2017).

[15] H.-P. Chou, Y.-S. Chang, S.-K. Chen, and J.-W. Yeh, Mater. Sci. Eng. B **163**, 184 (2009).

[16] W.-R. Wang, W.-L. Wang, S.-C. Wang, Y.-C. Tsai, C.-H. Lai, and J.-W. Yeh, Intermetallics **26**, 44 (2012).

[17] G. Anand, R. Goodall, and C. L. Freeman, Scr. Mater. **124**, 90 (2016).

[18] H. Feng, Z. Wang, Y. Li, Q. Wu, J. Li, J. Wang, and C. T. Liu, Sci. Rep. **6**, 34628 (2016).

[19] S. Huang, W. Li, X. Li, S. Schönecker, L. Bergqvist, E. Holmström, L. K. Varga, and L. Vitos, Mater. Design **103**, 71 (2016).

[20] H. Feng, Z. Wang, Q. Wu, J. Li, J. Wang, and C. T. Liu, Scr. Mater. **126**, 15 (2017).

[21] T. Huang, L. Jiang, C. Zhang, H. Jiang, Y. Lu, and T. Li, Sci. China: Technol. Sci. **61**, 117 (2018).

[22] E. Holmström, R. Lizárraga, D. Linder, W. Salmasi, A. Wang, B. Kaplan, H. Mao, H. Larsson, and L. Vitos, Appl. Mater. Today **12**, 322 (2018).

[23] H. Jobs and C. Balhausen, Vertrauensartzt und Krankenkasse **8**, 142 (1940).

[24] National Institutes of Health, Technical Report No. 14-5923, National Toxicology Program, U.S. Department of Health and Human Services, 2013.

[25] A. Linna, P. Oksa, K. Groundstroem, M. Halkosaari, P. Palmroos, S. Huikko, and J. Uitti, Occup. Environ. Med. **61**, 877 (2004).

[26] D. H. E. Persson, S. Jacobson, and S. Hogmark, Wear **255**, 498 (2003).

[27] L. Tian, R. Lizárraga, H. Larsson, E. Holmström, and L. Vitos, Acta Mater. **136**, 215 (2017).

[28] B. Bhushan, *Modern Tribology Handbook* (CRC, Boca Raton, 2001).

[29] H. M. Tawancy, Metallogr. Microstruct. Anal. **7**, 288 (2018).

[30] A. Love, S. Luyckx, and N. Sacks, J. Alloys Compd. **489**, 465 (2010).

[31] M. G. Poletti, G. Fiore, F. Gili, D. Mangherini, and L. Battezzati, Mater. Des. **115**, 247 (2017).

[32] P. Hohenberg and W. Kohn, Phys. Rev. **136**, B864 (1964).

[33] W. Kohn and L. Sham, Phys. Rev. **140**, A1133 (1965).

[34] L. Vitos, H. L. Skriver, B. Johansson, and J. Kollár, Comput. Mater. Sci. **18**, 20 (2000).

[35] L. Vitos, Phys. Rev. B **64**, 014107 (2001).

[36] L. Vitos, I. A. Abrikosov, and B. Johansson, Phys. Rev. Lett. **87**, 156401 (2001).

[37] L. Vitos, *Computational Quantum Mechanics for Materials Engineers: The EMTO Method and Applications* (Springer-Verlag, London, 2007).

[38] *Lectures on Methods of Electronic Structure Calculations*, edited by V. Kumar, A. Andersen, and O. K. Mookerjee (World Scientific, Singapore, 1995).

[39] O. K. Andersen, C. Arcangeli, R. Tank, T. Saha-Dasgupta, G. Krier, O. Jepsen, and I. Dasgupta, in *MRS Proceedings* (Cambridge University Press, Cambridge, UK, 1997), Vol. 491, p. 3.

[40] J. P. Perdew, K. Burke, and M. Ernzerhof, Phys. Rev. Lett. **77**, 3865 (1996).

[41] P. Soven, Phys. Rev. **156**, 809 (1967).

[42] D. W. Taylor, Phys. Rev. **156**, 1017 (1967).

[43] B. L. Gyorffy, Phys. Rev. B **5**, 2382 (1972).

[44] D. D. Johnson, D. M. Nicholson, F. J. Pinski, B. L. Gyorffy, and G. M. Stocks, Phys. Rev. Lett. **56**, 2088 (1986).

[45] D. D. Johnson, D. M. Nicholson, F. J. Pinski, B. L. Györffy, and G. M. Stocks, Phys. Rev. B **41**, 9701 (1990).

[46] D. D. Johnson and F. J. Pinski, Phys. Rev. B **48**, 11553 (1993).

[47] Y. Ikeda, B. Grabowski, and F. Körmann, Mater. Charact. (2018), doi: 10.1016/j.matchar.2018.06.019.

[48] Z. W. Lu, S. H. Wei, and A. Zunger, Phys. Rev. B **45**, 10314 (1992).

[49] G.-S. Wang, E. K. Delczeg-Czirjak, Q.-M. Hu, K. Kokko, B. Johansson, and L. Vitos, J. Phys.: Condens. Matter **25**, 085401 (2013).

[50] L.-Y. Tian, Q.-M. Hu, R. Yang, J. Zhao, B. Johansson, and L. Vitos, J. Phys.: Condens. Matter **27**, 315702 (2015).

[51] F. Tian, L. Delczeg, N. Chen, L. K. Varga, J. Shen, and L. Vitos, Phys. Rev. B **88**, 085128 (2013).

[52] S. Huang, A. Vida, D. Molnár, K. Kádas, E. Varga, L. K. Holmstrom, and L. Vitos, Appl. Phys. Lett. **107**, 251906 (2015).

[53] J. Kollár, L. Vitos, and H. Skriver, in *Electronic Structure and Physical Properies of Solids* (Springer, New York, 2000), pp. 85–114.

[54] L. Vitos, J. Kollár, and H. L. Skriver, Phys. Rev. B **55**, 13521 (1997).

[55] B. Gyorffy, A. Pindor, J. Staunton, G. Stocks, and H. Winter, J. Phys. F: Met. Phys. **15**, 1337 (1985).

[56] R. Lizárraga, F. Pan, L. Bergqvist, E. Holmström, and L. Vitos, Sci. Rep. **7**, 3778 (2017).

[57] See Supplemental Material at http://link.aps.org/supplemental/10.1103/PhysRevMaterials.2.094407 for the energy contours for $(CoCrFeNi)_{1-x}W_x$.

[58] T. Nishizawa and K. Ishida, Bull. Alloy Phase Diagrams **4**, 387 (1983).

[59] C. Niu, C. R. LaRosa, J. Miao, M. J. Mills, and M. Ghazisaeidi, Nat. Commun. **9**, 1363 (2018).

[60] P. Tolédano, G. Krexner, M. Prem, H. P. Weber, and V. P. Dmitriev, Phys. Rev. B **64**, 144104 (2001).

[61] D. Ma, B. Grabowski, F. Körmann, J. Neugebauer, and D. Raabe, Acta Mater. **100**, 90 (2015).

[62] C. Niu, A. J. Zaddach, A. A. Oni, X. Sang, J. W. Hurt III, J. M. LeBeau, C. C. Koch, and D. L. Irving, Appl. Phys. Lett. **106**, 161906 (2015).

[63] W. Schedler, *Hartmetallen für den Praktiker* (VDI-Verlag GmbH, Düsseldorf, 1998).

[64] B. Jansson and J. Qvick, in *Proceedings of the 16th International Plansee Seminar* (Plansee AG, Reutte, Austria, 2005), Vol. 2, pp. 1197–1206.

[65] Y.-F. Kao, S.-K. Chen, T.-J. Chen, P.-Ch. Chu, J.-W. Yeh, and S.-J. Lin, J. Alloys Compd. **509**, 1607 (2011).

[66] M. Lucas, D. Belyea, C. Bauer, N. Bryant, E. Michel, Z. Turgut, S. O. Leontsev, J. Horwath, S. L. Semiatin, M. E. McHenry *et al.*, J. Appl. Phys. **113**, 17A923 (2013).

[67] S. Huang, E. Holmström, O. Eriksson, and L. Vitos, Intermetallics **95**, 80 (2018).

[68] F. Körmann, D. Ma, D. D. Belyea, M. S. Lucas, C. W. Miller, B. Grabowski, and M. H. F. Sluiter, Appl. Phys. Lett. **107**, 142404 (2015).